



Detection of 2-mm-long strained section in silica fiber using slope-assisted Brillouin optical correlation-domain reflectometry

Heeyoung Lee*, Yosuke Mizuno, and Kentaro Nakamura

Institute of Innovative Research, Tokyo Institute of Technology, Yokohama 226-8503, Japan

*E-mail: hylee@sonic.pi.titech.ac.jp

Received October 25, 2017; accepted November 28, 2017; published online December 27, 2017

Slope-assisted Brillouin optical correlation-domain reflectometry is a single-end-access distributed Brillouin sensing technique with high spatial resolution and high-speed operation. We have recently discovered its unique feature, that is, strained or heated sections even shorter than nominal resolution can be detected, but its detailed characterization has not been carried out. Here, after experimentally characterizing this “beyond-nominal-resolution” effect, we show its usefulness by demonstrating the detection of a 2-mm-long strained section along a silica fiber. We also demonstrate the detection of a 5-mm-long heated section along a polymer optical fiber. The lengths of these detected sections are smaller than those of the other demonstrations reported so far. © 2018 The Japan Society of Applied Physics

Optical fiber sensing based on Brillouin scattering¹⁾ can provide information on the distributions of strain and temperature change, and is regarded as a promising technique for structural health monitoring. These days, with enhanced spatial resolution, not only civil infrastructures but also much smaller structures, such as optical waveguides, are focused on as sensing targets. Hence, many types of Brillouin-based measurement schemes have been developed, such as Brillouin optical time-domain reflectometry (BOTDR),^{2–5)} Brillouin optical frequency-domain reflectometry (BOFDR),⁶⁾ Brillouin optical correlation-domain reflectometry (BOCDR),^{7–10)} Brillouin optical time-domain analysis (BOTDA),^{11–15)} Brillouin optical frequency-domain analysis (BOFDA),^{16–18)} and Brillouin optical correlation-domain analysis (BOCDA).^{19–23)} While each scheme has its own merit and demerit, BOCDR is the only technique that operates by inherently one-end light injection and has high spatial resolution and cost efficiency, although it suffers from the trade-off relationship between the spatial resolution and the measurement range.

A number of BOCDR configurations have been implemented to improve the performance^{24–27)} since the first development of its original configuration.⁷⁾ As for the operating speed, the sampling rate of BOCDR has been limited to 19 Hz,⁸⁾ resulting in the difficulty in real-time distributed measurement. In 2016, however, we developed two high-speed configurations of BOCDR: phase-detected BOCDR²⁸⁾ and slope-assisted (SA-) BOCDR.²⁹⁾ In phase-detected BOCDR, the Brillouin gain spectrum (BGS) is converted to time-domain signal, and it is approximated by a sinusoidal waveform, the phase delay of which is directly obtained. By this technique, a 100 kHz sampling rate was achieved, and real-time distributed strain sensing was demonstrated. However, the limited strain dynamic range was a major problem, although some efforts to mitigate this limitation have been conducted.³⁰⁾ Thus, here we focus on SA-BOCDR.

In SA-BOCDR, the spectral power of the BGS is used to obtain the Brillouin frequency shift (BFS) by exploiting their one-to-one correspondence. The basic operations of SA-BOCDR have been demonstrated using not only silica glass optical fibers²⁹⁾ but also polymer optical fibers (POFs).³¹⁾ When POFs were used, 100-mm-long strained and heated sections were successfully detected.³²⁾ Recently, the relationship between the final system output (i.e., power-change distribution) and the actual BFS distribution has been inves-

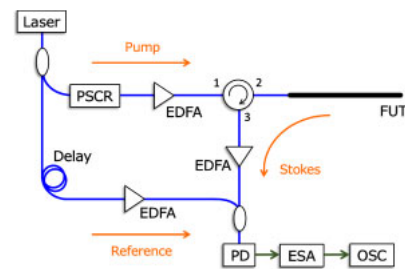


Fig. 1. (Color online) Experimental setup for SA-BOCDR. EDFA: erbium-doped fiber amplifier, ESA: electrical spectrum analyzer, FUT: fiber under test, OSC: oscilloscope, PD: photo diode, PSCR: polarization scrambler.

tigated.³³⁾ In addition, it has been proved that, even when the strained (or heated) section is shorter than the nominal spatial resolution, some shift in the power change can be observed.³³⁾ Although this “beyond-nominal-resolution” effect unique to SA-BOCDR is very attractive for practical applications, no detailed characterization has been performed yet.

In this work, first, we experimentally characterize the beyond-nominal-resolution effect of SA-BOCDR using a silica single-mode fiber (SMF). We find that a strained section that is over 50 times shorter than the nominal spatial resolution can be detected. Then, we show the usefulness of the beyond-nominal-resolution effect by detecting a 2-mm-long strained section along a silica SMF and a 5-mm-long heated section along a POF. These values are smaller than the world records previously reported, which are 3³⁴⁾ and 100 mm³²⁾ for a silica SMF and a POF, respectively [both values were restricted by the signal-to-noise ratios (SNRs) of the systems].

Figure 1 shows the experimental setup of SA-BOCDR used in the experiment. It is basically the same as that reported in our literature,²⁹⁾ to which reference should be made for a detailed explanation. A laser diode at 1550 nm with a bandwidth of ~ 1 MHz was used as a light source. Throughout the experiment in this work, the video and resolution bandwidths of the electrical spectrum analyzer (ESA) were set to 3 kHz and 10 MHz, respectively, while the repetition rate was 100 Hz. Note that a polarization scrambler was inserted in the pump path in this setup, but it could be inserted immediately after the laser output before an optical coupler.

First, to characterize the beyond-nominal-resolution effect, we employed a 14.0-m-long silica SMF as a fiber under test (FUT). The output light from a laser was amplified to ~ 25

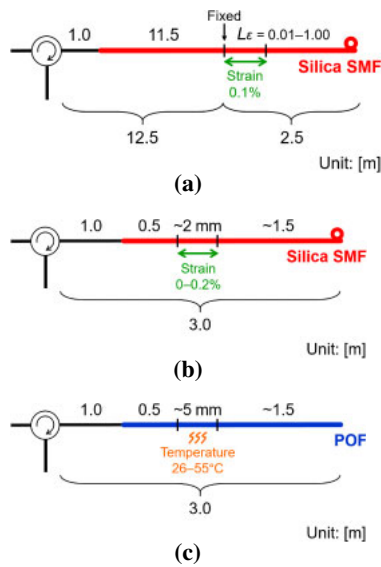


Fig. 2. (Color online) (a) Structure of a silica SMF under test. The length of the strained section L_e was set to 0.01, 0.02, 0.05, 0.10, 0.20, 0.50, and 1.00 m. (b) Structure of a silica SMF under test, which was locally strained for 0, 0.10, 0.15, and 0.20%. (c) Structure of a POF under test, which was locally heated to 26, 35, 45, and 55 °C.

dBm using an erbium-doped fiber amplifier (EDFA) and injected into the FUT. The BFS of the FUT was 10.89 GHz at 1.55 μm at 26 °C (room temperature). The open end of the FUT was bent to suppress the Fresnel reflection. The spectral power change at 10.87 GHz (determined by differentiating the BGS²⁹) was monitored using an oscilloscope (OSC). The modulation amplitude Δf and the modulation frequency f_m were set to 0.19 GHz and 5.10–5.26 MHz, respectively, leading to the nominal spatial resolution of 1.01 m and the measurement range of 20.1 m, calculated using Eqs. (15) and (16) in Ref. 8. A strain of 0.1% was applied to 0.01-, 0.02-, 0.05-, 0.10-, 0.20-, 0.50-, and 1.00-m-long sections of the FUT, as shown in Fig. 2(a). When the length of the strained section was changed, the position of its proximal end was fixed. Averaging was performed 512 times on the OSC to obtain a higher SNR. The number of sampling points was 2500.

Subsequently, exploiting the beyond-nominal-resolution effect, we attempted to detect the shortest-ever strained and heated sections along a silica SMF and a POF. In this experiment, we injected ~28 dBm light to the FUTs to enhance the measurement sensitivity,³⁵ and averaging was performed 1024 times. The number of sampling points was 2500. To begin with, as an FUT, we employed a 2.0-m-long silica SMF, the BFS of which was 10.85 GHz at room temperature. We applied strains of 0.10, 0.15, and 0.20% to a 2-mm-long section (fixed on translation stages using epoxy glue; ~55 times shorter than the nominal spatial resolution; see below), as depicted in Fig. 2(b). The nominal spatial resolution and the measurement range were 0.11 and 7.64 m (modulation amplitude Δf : 0.67 GHz; modulation frequency f_m : 13.45–13.54 MHz), respectively. The change in the spectral power at 10.84 GHz was observed using the OSC. Then, a 2.0-m-long perfluorinated graded-index (PFGI-) POF³⁶ (core diameter: 50 μm ; propagation loss at 1.55 μm : 0.25 dB/m; BFS at room temperature: 2.75 GHz) was used as an FUT. A 5-mm-long section was heated to 35, 45, and 55 °C [see Fig. 2(c)]. The modulation amplitude Δf and the modulation frequency

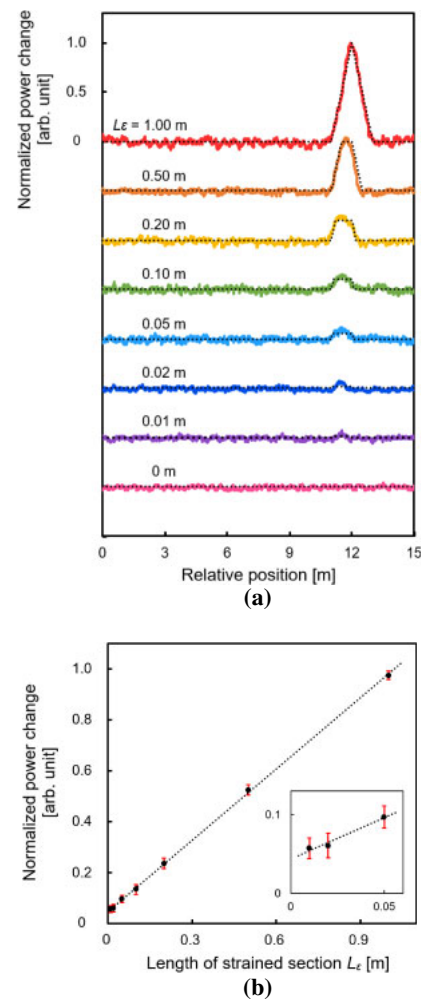


Fig. 3. (Color online) (a) Normalized power-change distributions measured when the length of the strained section L_e was reduced from 1.00 to 0.01 m; each distribution was shifted by 0.5. The dotted lines indicate the theoretical trends. (b) Maximal power changes plotted as a function of L_e . The error bars are calculated as standard deviations of the signal fluctuations at nonstrained sections. The dotted line is a linear fit. The inset shows the magnified view at L_e shorter than 0.1 m.

f_m were set to 0.69 GHz and 24.70–24.84 MHz, respectively, resulting in the nominal spatial resolution of 0.21 m and the measurement range of 4.5 m.⁸⁾ Note that the length of the heated section was over 40 times smaller than the nominal spatial resolution. The change in the spectral power at 2.78 GHz was monitored.

The power-change distributions measured when the length of the strained section L_e was reduced from 1.00 to 0.01 m are shown in Fig. 3(a). Note that the nominal spatial resolution was 1.01 m throughout the measurement. The vertical axis was normalized so that the maximal power change became 1 when L_e was 1.00 m. Each distribution was displayed with a vertical interval of 0.5. When L_e was 1.00 m, the power-change distribution showed a triangular shape, which is natural considering the operating mechanism of SA-BOCDR.³³ As L_e decreased, the maximal power change also decreased. When L_e was 0.02 m, the power change was still clearly detected, but it became almost comparable to the signal fluctuations (calculated standard deviation: 0.06) when L_e was 0.01 m. Thus, under this experimental condition, a strained section that is over 50 times shorter than the nominal spatial resolution was shown to be detectable. Figure 3(b)

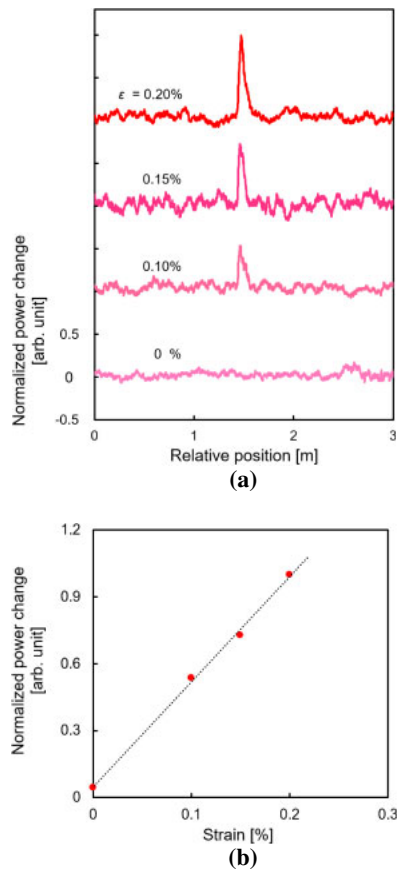


Fig. 4. (Color online) (a) Normalized power-change distributions along a silica SMF measured at four strains. Each distribution was shifted by 1. (b) Maximal power changes plotted as a function of strain. The dotted line is a linear fit.

shows the normalized maximal power change plotted as a function of L_e . The error bars were standard deviations of the signal fluctuations at nonstrained sections. The maximal power change decreased almost linearly with decreasing L_e , which agrees well with the theory.³³⁾ The observed length of the nonzero-power-change section was almost equal to the sum of the strained length L_e and the nominal spatial resolution, which also agrees with the theory³³⁾ (quantitative evaluation is difficult because of the low SNR when L_e is short).

Next, exploiting the beyond-nominal-resolution effect verified above, we attempted to detect the shortest-ever strained and heated sections along a silica SMF and a POF. Figure 4(a) shows the normalized power-change distributions measured when strains of 0.10, 0.15, and 0.20% were applied to a 2-mm-long section of the silica SMF. The local power changes corresponding to the strain were observed at the correct position. The lengths of the power-changed sections appeared to be much larger than 2 mm; in theory,³³⁾ they should be almost the same as the nominal resolution (0.11 m), which moderately agrees with the measured results. The maximal normalized power change of each distribution in Fig. 4(a) was plotted as a function of applied strain in Fig. 4(b). With increasing strain, the power-change also increased almost linearly, which indicates that the magnitude of the strain can be correctly measured in this strain range. Then, we performed a similar experiment using the POF. The normalized power-change distributions measured when the 5-mm-long section was heated to 26 (room temperature),

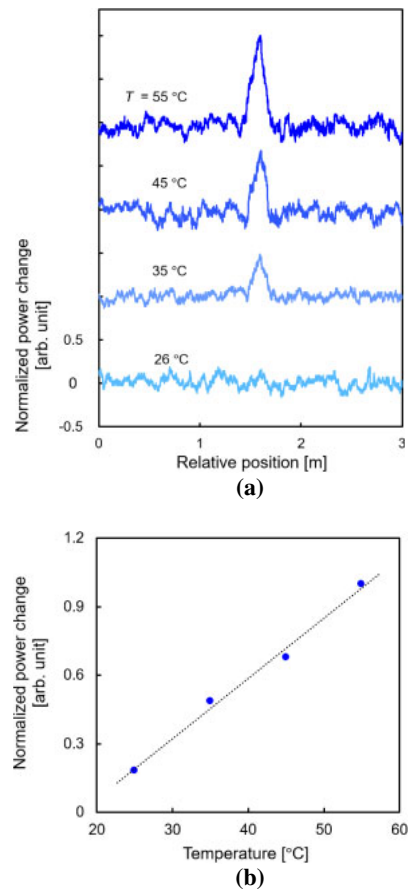


Fig. 5. (Color online) (a) Normalized power-change distributions along a POF measured at four temperatures. Each distribution was shifted by 1. (b) Maximal power changes plotted as a function of temperature. The dotted line is a linear fit.

35, 45, and 55 °C are shown in Fig. 5(a). The abrupt power changes were observed at the correct position along the POF. The lengths of the power-changed sections moderately agreed with the nominal resolution (0.21 m). The magnitude of the maximal power change was proportional to the temperature change as shown in Fig. 5(b), indicating the potential feasibility of distributed temperature sensing.

Hereafter, we discuss the unique features of the beyond-nominal-resolution effect of SA-BOCDR in detail. The first discussion is regarding the measurement capability of the location, length, and magnitude of applied strain, when the strain is shorter than the nominal spatial resolution. The strain location can be derived from the system output as the center of the nonzero-power-change section, and the strained length can be given by subtracting the nominal spatial resolution from the length of the nonzero-power-change section, as already mentioned. The strain magnitude can also be given by the maximal power change and the ratio of the strained length to the nominal spatial resolution. Thus, if the SNR of the system is sufficiently high, these three parameters of strain can be theoretically obtained from the measured power-change distribution, although the SNR may not be sufficiently high in most practical cases.

Next, we discuss the validity of claiming that the 2-mm-long strained SMF section and the 5-mm-long heated POF section were detected. When a 2-mm-long strain was applied to the SMF using epoxy glue, unintended strain distribution

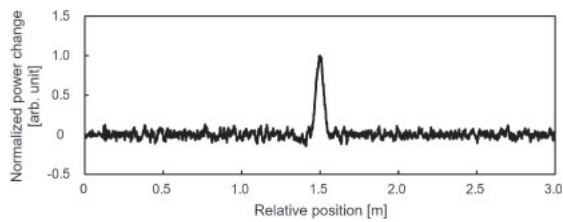


Fig. 6. Normalized power-change distribution along a silica SMF. A 2-mm-long silica SMF with different BFS was, as pseudostrain, spliced between two silica SMFs.

was inevitably induced along the SMF inside the glue. This may result in a practically longer strain to be measured. To avoid this effect and to prove that the 2-mm-long strain was truly detected, we performed an additional experiment. By splicing a 2-mm-long SMF with a different BFS (11.02 GHz at room temperature), we induced pseudostrain with a length of exactly 2 mm and measured the power-change distribution [the other experimental conditions were the same as those used in Fig. 4(a)]. The result shown in Fig. 6 clearly indicates that the 2-mm-long pseudostrain was truly detected. As for the temperature measurement, it is difficult to completely avoid the influence of the thermal conduction, and the detected heated section may be slightly longer than 5 mm; however, the conclusion that this system has the capability to detect a 2-mm-long section with a different BFS remains true.

The third discussion is regarding the limitation of the detectable strained length. In this experiment, it was restricted to 2 mm because of the deteriorated SNR. Therefore, the limitation could be enhanced by improving the SNR by using higher-power incident light or by applying a larger strain. For instance, in Fig. 4(a), a clear peak (which can be discriminated from the noise floor even when the power-change becomes half) was observed at 0.2% strain; this may indicate that strain with a length of less than half of 2 mm, namely of sub-millimeter length, can be potentially detected by SA-BOCDR.

Lastly, we discuss the possibility of employing this technique in other types of Brillouin sensors. We consider that the beyond-nominal-resolution effect can also be given to BOCDA systems, because they work on a similar principle of BOCDA (the final system output of BOCDA can be expressed by the same mathematical forms as that of BOCDA).⁸⁾ As BOCDA exploits stimulated Brillouin scattering, which is much larger than spontaneous scattering, we predict that the beyond-nominal-resolution effect of SA-BOCDA will have higher performance than SA-BOCDR and deserve developing in the future, despite its shortcomings in terms of the two-end-access nature and the complexity of the setup.

In conclusion, first, we experimentally characterized the “beyond-nominal-resolution” effect of SA-BOCDR using the silica SMF. When the nominal spatial resolution was constant, the measured maximal power change decreased almost linearly with decreasing length of the strained section. Even when the strained length was over 50 times shorter than the nominal spatial resolution, power change was still clearly observed at the correct position. Subsequently, by exploiting this effect, we demonstrated detection of the 2-mm-long strained section in the silica SMF and a 5-mm-long heated section in the POF. In both cases, the power-change distributions at four different strains and temperatures were measured, and the maximal power changes at each distribution

increased almost linearly with increasing strain and temperature. These results indicate that, even when the strained (or heated) section is much shorter than the nominal spatial resolution, if the SNR is sufficiently high, its length and the magnitude of the applied strain (or temperature change) can be potentially calculated from the measured power-change distribution. Thus, we anticipate that this work, which has proven the capability of detecting extremely short strained/heated sections along optical fibers, will greatly enhance the practical applicability of SA-BOCDR in the near future.

Acknowledgments This work was supported by JSPS KAKENHI Grant Numbers 17H04930 and 17J07226, and by research grants from the Japan Gas Association, the ESPEC Foundation for Global Environment Research and Technology, the Association for Disaster Prevention Research, the Fujikura Foundation, and the Japan Association for Chemical Innovation.

- 1) G. P. Agrawal, *Nonlinear Fiber Optics* (Academic Press, San Diego, CA, 1995).
- 2) T. Kurashima, T. Horiguchi, H. Izumita, S. Furukawa, and Y. Koyamada, *IEICE Trans. Commun.* **E76-B**, 382 (1993).
- 3) W. Li, X. Bao, Y. Li, and L. Chen, *Opt. Express* **16**, 21616 (2008).
- 4) D. Iida and F. Ito, *J. Lightwave Technol.* **26**, 417 (2008).
- 5) F. Wang, W. Zhan, X. Zhang, and Y. Lu, *J. Lightwave Technol.* **31**, 3663 (2013).
- 6) A. Minardo, R. Bernini, R. Ruiz-Lombera, J. Mirapeix, J. M. Lopez-Higuera, and L. Zeni, *Opt. Express* **24**, 29994 (2016).
- 7) Y. Mizuno, W. Zou, Z. He, and K. Hotate, *Opt. Express* **16**, 12148 (2008).
- 8) Y. Mizuno, W. Zou, Z. He, and K. Hotate, *J. Lightwave Technol.* **28**, 3300 (2010).
- 9) N. Hayashi, Y. Mizuno, and K. Nakamura, *IEEE Photonics J.* **6**, 6802807 (2014).
- 10) N. Hayashi, Y. Mizuno, and K. Nakamura, *Appl. Phys. Express* **7**, 112501 (2014).
- 11) T. Horiguchi and M. Tateda, *J. Lightwave Technol.* **7**, 1170 (1989).
- 12) M. A. Soto, G. Bolognini, F. D. Pasquale, and L. Thévenaz, *Opt. Lett.* **35**, 259 (2010).
- 13) A. Minardo, R. Bernini, and L. Zeni, *Opt. Express* **19**, 19233 (2011).
- 14) Y. Dong, D. Ba, T. Jiang, D. Zhou, H. Zhang, C. Zhu, Z. Lu, H. Li, L. Chen, and X. Bao, *IEEE Photonics J.* **5**, 2600407 (2013).
- 15) Y. Peled, A. Motil, I. Kressel, and M. Tur, *Opt. Express* **21**, 10697 (2013).
- 16) D. Garus, T. Gogolla, K. Krebber, and F. Schliep, *Opt. Lett.* **21**, 1402 (1996).
- 17) D. Garus, T. Gogolla, K. Krebber, and F. Schliep, *J. Lightwave Technol.* **15**, 654 (1997).
- 18) R. Bernini, A. Minardo, and L. Zeni, *IEEE Photonics J.* **4**, 48 (2012).
- 19) K. Hotate and T. Hasegawa, *IEICE Trans. Electron.* **E83-C**, 405 (2000).
- 20) W. Zou, C. Jin, and J. Chen, *Appl. Phys. Express* **5**, 082503 (2012).
- 21) C. Zhang, M. Kishi, and K. Hotate, *Appl. Phys. Express* **8**, 042501 (2015).
- 22) W. Zou, Z. He, and K. Hotate, *IEEE Sens. J.* **14**, 244 (2014).
- 23) R. K. Yamashita, M. Kishi, and K. Hotate, *Appl. Phys. Express* **10**, 042501 (2017).
- 24) Y. Mizuno, Z. He, and K. Hotate, *Opt. Express* **18**, 5926 (2010).
- 25) N. Hayashi, Y. Mizuno, and K. Nakamura, *IEEE Photonics J.* **7**, 6800407 (2015).
- 26) Y. Mizuno, Z. He, and K. Hotate, *Opt. Commun.* **283**, 2438 (2010).
- 27) N. Hayashi, Y. Mizuno, and K. Nakamura, *IEEE Photonics J.* **6**, 6803108 (2014).
- 28) Y. Mizuno, N. Hayashi, H. Fukuda, K. Y. Song, and K. Nakamura, *Light: Sci. Appl.* **5**, e16184 (2016).
- 29) H. Lee, N. Hayashi, Y. Mizuno, and K. Nakamura, *IEEE Photonics J.* **8**, 6802807 (2016).
- 30) Y. Mizuno, N. Hayashi, H. Fukuda, and K. Nakamura, *Jpn. J. Appl. Phys.* **56**, 072501 (2017).
- 31) H. Lee, N. Hayashi, Y. Mizuno, and K. Nakamura, *J. Lightwave Technol.* **35**, 2306 (2017).
- 32) N. Hayashi, Y. Mizuno, and K. Nakamura, *J. Lightwave Technol.* **32**, 3999 (2014).
- 33) H. Lee, N. Hayashi, Y. Mizuno, and K. Nakamura, *Opt. Express* **24**, 29190 (2016).
- 34) K. Y. Song, Z. He, and K. Hotate, *Opt. Lett.* **31**, 2526 (2006).
- 35) H. Lee, Y. Mizuno, and K. Nakamura, *Sens. Actuators A* **268**, 68 (2017).
- 36) Y. Koike and M. Asai, *NPG Asia Mater.* **1**, 22 (2009).